Research article

Kaempferol sophoroside glucoside mitigates acetaminophen-induced hepatotoxicity: Role of Nrf2/NF-κB and JNK/ASK-1 signaling pathways

Gamal A. Mohamed [a,**], Dina S. El-Agamy [b], Hossam M. Abdallah [a], Ikhlas A. Sindi [c], Mohammed A. Almogaddam [d], Abdulrahim A. Alzain [d], Yusra Saleh Andijani [e], Sabrin R.M. Ibrahim [f,g,*]

[a] Department of Natural Products and Alternative Medicine, Faculty of Pharmacy, King Abdulaziz University, Jeddah, 21589, Saudi Arabia
[b] Department of Pharmacology and Toxicology, Faculty of Pharmacy, Mansoura University, Mansoura, 35516, Egypt
[c] Department of Biology, Faculty of Science, King Abdulaziz University, Jeddah, 21589, Saudi Arabia
[d] Department of Pharmaceutical Chemistry, Faculty of Pharmacy, University of Gezira, Wad Madani, 21111, Sudan
[e] Department of Pharmacology and Toxicology, College of Pharmacy, Taibah University, Al-Madinah Al-Munawwarah, 30078, Saudi Arabia
[f] Department of Chemistry, Preparatory Year Program, Batterjee Medical College, Jeddah, 21442, Saudi Arabia
[g] Department of Pharmacognosy, Faculty of Pharmacy, Assiut University, Assiut, 71526, Egypt

ARTICLE INFO

ABSTRACT

APAP (Acetaminophen)-induced hepatic injury is a major public health threat that requires continuous searching for new effective therapeutics. KSG (Kaempferol-3-sophoroside-7-glucoside) is a kaempferol derivative that was separated from plant species belonging to different genera. This study explored the protective effects of KSG on ALI (acute liver injury) caused by APAP overdose in mice and elucidated its possible mechanisms. The results showed that KSG pre-treatment alleviated APAP-induced hepatic damage as it reduced hepatic pathological lesions as well as the serum parameters of liver injury. Moreover, KSG opposed APAP-associated oxidative stress and augmented hepatic antioxidants. KSG suppressed the inflammatory response as it decreased the genetic and protein expression as well as the levels of inflammatory cytokines. Meanwhile, KSG enhanced the mRNA expression and level of anti-inflammatory cytokine, IL-10 (interleukin-10). KSG repressed the activation of NF-κB (nuclear-factor kappa-B), besides it promoted the activation of Nrf2 signaling. Additionally, KSG markedly hindered the elevation of ASK-1 (apoptosis-signal regulating-kinase-1) and JNK (c-Jun-N-terminal kinase). Furthermore, KSG suppressed APAP-induced apoptosis as it decreased the level and expression of Bax (BCL2-associated X-protein), and caspase-3 concurrent with an enhancement of anti-apoptotic protein, Bcl2 in the liver. More thoroughly, Computational studies reveal indispensable binding affinities between KSG and Keap1 (Kelch-like ECH-associated protein-1), ASK1 (apoptosis signal-regulating kinase-1), and JNK1 (c-Jun N-terminal protein kinase-1) with distinctive tendencies for selective inhibition. Taken together, our data showed the hepatoprotective capacity of KSG against APAP-

* Corresponding author.
** Corresponding author.

produced ALI via modulation of Nrf2/NF-κB and JNK/ASK-1/caspase-3 signaling. Henceforth, KSG could be a promising hepatoprotective candidate for ALI.

1. Introduction

Acetaminophen (APAP) is among the most popular used analgesics/antipyretic agents worldwide. As it is well tolerated in therapeutic doses, it is found in many prescriptions and over-the-counter medications. However, as a result of its widespread availability, patients may be exposed intentionally or unintentionally to APAP overdose which results in extensive liver injury or failure. In the United States and several other Western countries, APAP toxicity constitutes roughly half of all acute liver failure cases. Till now, NAC (N-acetylcysteine) is the only approved antidote for APAP-induced hepatotoxicity despite its narrow therapeutic window [1–3].

The pathogenic mechanisms of APAP-produced ALI (acute-liver injury) are complicated and include crosstalk between oxidant stress, inflammation, mitochondrial malfunction, endoplasmic reticulum stress, and autophagy [4–6]. Cytochrome-P450 2E1 metabolizes APAP to generate an extremely active metabolite, NAPQI (N-acetyl-p-benzoquinone-imine) that rapidly conjugates with the endogenous antioxidant GSH (glutathione). Following APAP overdose, depletion of the cellular GSH pool occurs, followed by subsequent accumulation of NAPQI which binds with other cellular proteins to form cytotoxic arylated proteins that create a state of oxidative stress, eventual hepatocyte death and massive hepatic necrosis [7]. Excessive oxidative stress results in the activation of inflammatory signaling of the transcription factor, NF-κB (nuclear-factor kappa-B) which is normally present in the cytosol in an inactive state. Many studies documented the activation, nuclear translocation of NF-κB-p65 and subsequent induction of the transcription of some inflammatory genes as ILs (interleukins) and TNF-α (tumor-necrosis factor-α) following APAP overdose [8–10].

NAPQI-induced mitochondrial oxidant stress has been shown to trigger the activation of a MAPK (mitogen-activated-protein-kinase) kinases cascade, including ASK1 (apoptosis signal-regulating kinase-1), causing the JNK (c-Jun N-terminal-kinase) phosphorylation in the cytoplasm. In normal conditions, ASK-1 interacts with Trx (thioredoxin) to form an inactive complex. Following APAP overdose, the excessive generation of oxidative ROS (reactive oxygen species) and other inflammatory stimuli such as TNF-α can activate ASK-1, leading to JNK and p38 signaling pathways' activation that contributes to ALI [11,12]. P-JNK transfers to the mitochondria and causes the permeability transition pore to open, as well as the loss of the potential of the mitochondrial membrane, further mitochondrial dysfunction and the resultant release of apoptotic factors [2,13].

The crosstalk between inflammatory signaling and antioxidant regulators has been identified during APAP-induced ALI. The Nrf2 (nuclear-factor E2-related factor-2) a redox-sensitive transcription factor that modulates most of the defence proteins including the enzymes that synthesize GSH, has been involved in the development of APAP-produced hepatotoxicity [14]. Nrf2-deficient mice were extremely sensitive to APAP toxicity, whereas mice with constitutive Nrf2 activation were extremely resistant [15], while Nrf2 activation was documented to effectively protect against APAP-induced ALI [16,17].

Medicinal plants are established to have a substantial role in human healthcare not only as a treatment of various diseases but also to maintain good health conditions and well-being. It was estimated that more than two-thirds of the world's population depends on medicinal plants' uses in herbal medicine [18,19].

The well-established phytochemicals' health benefits and growing popularity of herbal medicine resulted in the development of several phytopharmaceutical and nutraceutical products that are utilized as therapeutic drugs for treating various illnesses and as nutritional supplements for promoting general well-being [20].

Various reports revealed the hepato-protection capacity of different phytoconstituents and/or plant-derived extracts on different hepatotoxin-induced liver injuries [21–23]. The plant extracts effectiveness was attributed to their antioxidant constituents such as flavonoids and phenolics.

Flavonoids are well-recognized, low-molecular-weight constituents that are vastly present in different plants and foods [24]. They are of health value as anti-inflammatory, antioxidant, anti-viral, anti-microbial, chemo-preventive, hepato-protective, anti-mutagenic, and anti-diabetic. In addition, their cellular key enzymes modulating capacity makes them an essential part of nutraceutical and pharmaceutical products [25–27]. Flavonoids such as quercetin, kaempferol, myricitrin, luteolin, malvidin, epicatechin, hesperetin, and apigenin were proven to be protective against liver injury through different actions such as controlling the Nrf2 signaling pathway, suppressing NLRP3-inflammasome, reducing NO and malondialdehyde, and prohibiting apoptosis, autophagy, and oxidative stress [25].

Kaempferol and its derivatives are abundant flavonoid glycosides in numerous plants [28]. It was reported that the dietary plants having kaempferol safeguard against different lethal disorders and organ-boosted oxidative injury by repressing apoptosis and inflammation and raising antioxidants in many tissues including the liver, brain, heart, and kidney [29]. Kaempferol demonstrated hepatoprotection capacity from oxidative stress-mediated liver injury using different models such as bromobenzene, alcohol, carbon tetrachloride, rifampicin, and APAP [29,30]. Its effect was mediated by prohibiting the GSH decrease and cytochrome-P450 2E1, increasing antioxidants, and repressing lipid peroxidation [31]. Kaempferol 3-sophoroside-7-glucoside is one of the kaempferol derivatives that was reported from plant species belonging to different genera such as *Hosta*, *Asplenium*, *Brassica*, *Sinapis*, *Lathyrus*, and, *Crocus* [32–35]. It is noteworthy that this compound has not been previously evaluated for its possible bioactivity.

Structural-based drug design harnesses the merits of computer sciences to shorten the journey of drug development and discovery [36]. For the fulfillment of such procedures, the three-dimensional structure of the protein should be preidentified, usually through homology modeling, X-ray crystallography, and nuclear magnetic resonance spectroscopy [37]. Following the identification of a binding site, a broad variety of chemical compounds can be screened for their binding affinity and interaction with the target protein's

active site based on how they interact sterically, hydrophobically, and electrostatically with the active site of a target protein [38]. The optimum allocation of SBDD (structure-based drug design) methodologies offers comprehensive information about the protein's active sites, understanding the active compound's molecular-level mechanism of action, and reviewing the kinetics and thermodynamics parameters utilized in target-ligand interaction [39].

In this regard, this study aimed to discover novel therapy strategies for APAP overdose using one of the kaempferol derivatives; KSG and elucidate the mechanisms of hepato-protective activities in rodent models.

2. Materials and methods

2.1. Materials

N-acetylcysteine (NAC) was dissolved in 0.9 % sterile saline before use (Sigma Aldrich- St. Louis- MO- USA). APAP was acquired as 10 mg/mL injectable ampoules (Perfalgan/Bristol/Myers Squibb/Victoria/Australia). KSG was provided by Chengdu Bio-purify Phytochemicals Ltd. (Chengdu city/Sichuan/China). KSG was suspended in 0.5 % CMC (carboxymethyl cellulose) just before use.

2.2. Experimental design

Male mice BALB/c (20–25g, 6–8 weeks old) were housed under humidity/temperature/light cycle standard conditions before and during the experimental period with unrestricted access to food and water.

APAP-induced hepatotoxicity was carried out as mentioned earlier [14,16]. Animals were randomly assigned (six groups, 6 mice each) to the following treatments: (**1**) Control (sterile saline with 0.5 % CMC), (**2**) KSG (100 mg/kg, orally) for 7 days, (**3**) APAP (0.5% CMC for 7 days then APAP (500 mg/kg, i.p.)), (**4**) KSG-50 + APAP (KSG 50 mg/kg/orally for 7 days, followed by APAP 500 mg/kg), (**5**) KSG-100 + APAP (KSG 100 mg/kg/orally for 7 days, followed by APAP 500 mg/kg), (**6**) NAC + APAP (NAC 100 mg/kg, orally for 7 days followed by APAP 500 mg/kg). This group is a positive group for determining KSG's hepatoprotective effectiveness. The KSG dose was chosen based on a pilot experiment in which four doses of KSG (5, 10, 50, and 100 mg/kg) were assessed against APAP-produced hepatic injury. The doses of KSG were chosen based on the positive results of serum parameters of hepatic injury and liver histopathology.

24 h after the APAP injection, mice were euthanized by cervical dislocation under anaesthesia with xylazine (10 mg/kg) and ketamine (75 mg/kg). blood samples were collected and centrifugated to obtain serum that was kept at – 80 °C for further analysis. Liver samples were harvested. A small piece of hepatic tissue was homogenized in PBS (phosphate-buffered saline) and centrifuged to get the supernatant for ELISA (enzyme-linked immunosorbent assays), oxidative stress, and antioxidant analysis. A piece of the liver's right lobe was immersed in 10 % neutral-buffered formalin and submitted for histological and immunohistochemical (IHC) analysis.

2.3. Histo-pathological and immuno-histochemical (IHC) analysis

Liver samples were dehydrated using ethanol and then embedded in paraffin. The blocks were sectioned and stained with hematoxylin-eosin (H&E). In random order, the specimen was blindly examined, and the pathologic lesions were recorded from 0 to 4 as stated previously [14].

For IHC, the liver paraffin sections were processed as formerly described [22,40]. Sections were immuno-stained using the primary antibodies: rabbit-poly-clonal antibody against IL-6 (1: 100), TNF-α (1:100), NF-κB p65 (1: 200), Bcl2 (1:200), Nrf2 (1: 200), and caspase-3 (1: 200) (Fisher-Scientific Inc.-Waltham-MA-USA; Elabscience-Biotechnology Inc.-Houston-TX-USA). DAB (dia-minobenzidine) was employed for visualization. Semiquantitative analysis was achieved using the image analysis software (ImageJ/NIH).

2.4. Biochemical analysis

Using UNICO® Model S1200 Spectrophotometer (UNICO Instruments C./NJ/USA), the serum levels of LDH (lactate-dehydroge-nase), ALP (alkaline phosphatase), aminotransferases (ALT, AST), and γ-GT (gamma-glutamyl transferase) were determined using commercial kits following the manufacturer's protocols (Human/Wiesbaden/Germany).

2.5. Lipid peroxidative markers and antioxidants

The levels of MDA (malondialdehyde), 4-HNE (4-Hydroxynonenal), GSH-px (glutathione-peroxidase), GST (glutathione-s-trans-ferase), GSH (glutathione), and SOD (super-oxide-dismutase) were estimated in the hepatic supernatants using the corresponding commercial assay kits (Bio-Diagnostic Co./Giza/Egypt).

2.6. Enzyme-linked immunosorbent assays (ELISA)

Levels of TNF-α, IL-6, IL-1β, ASK-1, JNK, Bcl2, Bax, caspase-3, and NF-κBp65 were assessed in the hepatic tissue' supernatants utilizing ELISA kits manufacturer's instructions. In the nuclear extract, Nrf2 binding activity was estimated as stated in the kit's guidelines (Active-Motif Inc.-Carlsbad -USA).

2.7. RT-PCR

Gene expression of TNF-α, IL-6, NF-κBp65, Nrf2, Bcl2, Bax, and caspase-3 was estimated using RT-PCR. Briefly, RNA extraction was done employing QIAzol reagent according to the provided instructions (Qiagen/Germany). The RNA concentration was determined using NanoDrop-2000 (Thermo-Scientific/USA). RNA Reverse transcription ($\approx$1 µg) was performed based on the protocol of the cDNA synthesis kit. RT-PCR was carried out employing the primers listed in Table S1. GAPDH (Glyceraldehyde-3-phosphate-dehydrogenase) was the control gene; and gene expression change was estimated using the $2^{-\Delta\Delta CT}$ method.

2.8. Data analysis

One-way ANOVA and then Tukey Kramer's multiple comparisons test were adopted for comparing multiple groups. Results were presented as mean $\pm$ SEM. GraphPad Prism (GraphPad Software/USA) was used to obtain the figures. <0.05 P value was referred to as significant.

2.9. Computational analysis

2.9.1. Protein preparation

Protein preparation is a crucial procedure for the issuance of the computational analysis reproducibility [41]. This process is solely focused on the normalization of stearic clashes in the protein structure and the optimization of hydrogen atoms and bonds. In this study, the structures of the rate-limiting proteins in ALI occurrence i.e., ASK-1 (PDB ID: 6E2N), Keap-1 (BDP ID: 7OFE), and JNK (BDP ID: 3PZE), were retrieved from the Protein-Data-Bank [42]. The three PDB structures were submitted to the protein preparation wizard of Schrodinger's Maestro 12.8 software package [43]. In subsequent, the proteins were preprocessed, this entails the addition of any missing hydrogens, the assignment of the bond orders in each amino acid, the deletion of any heteroatom or solvent molecule within 5 Å, the optimization of hydrogen bonds, and the creation of zero-ordered bonds to the metals [44]. In the follower step, the missing loops and/or chains were checked and added using Maestro's Prime module. Finally, the optimized structures were subjected to energy minimization by the prime module, and the energy parameters were derived from the OPLS forcefield [45].

2.9.2. Ligand preparation

The 2D structure for KSG was retrieved from the PubChem online database and prepared *via* the LigPrep module of Schrodinger. Herein, the module recruits the Epik software program for pKa prediction and protonation state generation for drug-like molecules which utilizes the SMARTS pattern of the selected compound to generate optimized Lewis's structure, moreover, Epik generates the possible tautomers protonation states of the molecule in the physiological PH (7 $\pm$ 2). Furthermore, the minimized three-dimensional assembly has been created [46].

2.9.3. Receptor Grid generation and molecular docking

For the sake of efficiency, the binding site identification before docking processes is inevitable. The receptor grid generator tool in Schrodinger's Maestro 12.8 software suite was employed to design a cubic grid based on the centroids of the co-crystalized ligand for the three studies proteins and the output files were preserved for the docking procedure [47].

Molecular docking is one of the most popular SBDD methodologies. The theory of molecular docking emphasizes upon the anticipation of binding affinity and ligand orientation at the target protein's active site [48]. Molecular docking software predicts the possible poses for the molecules through the implementation of software algorisms and indicates the intramolecular interaction of small molecules at the target protein's binding site to distinguish the ligand's binding strength with a target protein using mathematical scoring functions which is most often depends on the number of H bonds, binding energies, and potential hits found in the protein-ligand complex structure [37].

In this research, the molecular docking studies of KSG and the co-crystalized molecule for each protein were conducted using the GLIDE (Gride-based Ligand Docking with Energetics) platform provided by Schrodinger's Maestro 12.8. GLIDE module adopts Monte Carlo simulated annealing algorithms in the search for the conceivable ligand poses and scores the resultant poses using imperial scoring functions [36]. GLIDE proposed three distinct modes for docking which differ from one another in the extensiveness of sampling and the degree of freedom in the scoring function. High throughput virtual screening HTVS focuses on the selection of molecules that can geometrically fit into the active site with less comprehensiveness in the sampling process and a highly forgiving scoring function [49]. It is useful in reducing the number of molecules in large databases by nominating the most likely active molecules for further analysis. GLIDE Standard Precision SP mode offers better scoring and sampling processes. It employs the Glide SP score which is more coherent than the HTVS scoring function, however, the Glide SP score showcases some degree of softness since it is designed to identify the molecules that possess a reasonable propensity of binding even if the pose itself is imperfect [50,51].

GLIDE extra-precision XP mode represents the most concrete GLIDE docking model since it applies a wider docking funnel therefore more extensive sampling takes place. Furthermore, it uses Glide 4.0 XP score which applies numerous penalties to differentiate the active poses. XP score is calculated through **Equation (1)**, whereas, E(coul) scores the contribution of columbic (electrostatic) attraction, E(vdW) is the score of van der Wall forces, E(bind) is the score of the binding energy calculated in **Equation (2)** and based on the hydrophobic interaction between the protein and ligand atoms $E\left(hyd_{enclosure}\right)$ Neutral-Neutral HB $E\left(hb_{nn_{motif}}\right)$, Charged-Charged HB between the ligand and the receptor, π-stacking/π-cation contribution E(π), HB $E\left(h_{pair}\right)$ and hydrophobic

$\mathrm{E}\left(\mathrm{phobic_{pair}}\right)$ atom-atom pair energy [50,51] -.

$$\mathrm{XP\ GlideScore} = \mathrm{E(coul)} + \mathrm{E(vdW)} + \mathrm{E(bind)} + \mathrm{E(penalty)} \tag{1}$$

$$\mathrm{Ebind} = \mathrm{E(hyd_{enclosure})} + \mathrm{E}\left(\mathrm{hb_{nn_{motif}}}\right) + \mathrm{E}\left(\mathrm{hb_{cc_{motif}}}\right) + \mathrm{E(\pi)} + \mathrm{E}\left(\mathrm{h_{pair}}\right) + \mathrm{E}\left(\mathrm{phobic_{pair}}\right) \tag{2}$$

$$E(penalty) = E(disolv) + E(ligand_{strain}) \tag{3}$$

Equation (3) symbolizes the applied penalties E(penalty) for the generated poses where E(disolv) represents the desolvation penalties and $E(ligand_{strain})$ represents the penalties of strain energy of the generated poses. Considering these complex calculations plus egregious confirmational search, GLIDE XP excels over the other docking modes in terms of precision and credibility and precision. Upon this fact, XP docking was the chosen methodology to study the interactions between KSG and the selected proteins [52].

2.9.4. Insilco toxicity studies

Previous studies stated that nearly one-third of the newly discovered leads fail due to toxicological reasons. Drug-related toxicity is attributed to numerous causes, for example, off-target binding, impaired distribution and/or metabolism, the liberation of toxic byproducts, and plentiful interaction profile. Most of these toxicities are related to the chemical structure of the bioactive molecule i.e., the toxicity of a drug molecule is due to its possession of specific substructures [39]. The tracing of the toxic structure before lead optimization would dramatically increase the efficiency of the drug discovery process. It becomes attainable to detect these structures and their related toxicity by specific computational tools. Henceforth, we exploited the Pro Tox II web server to review the toxicological tendencies of KSG [53].
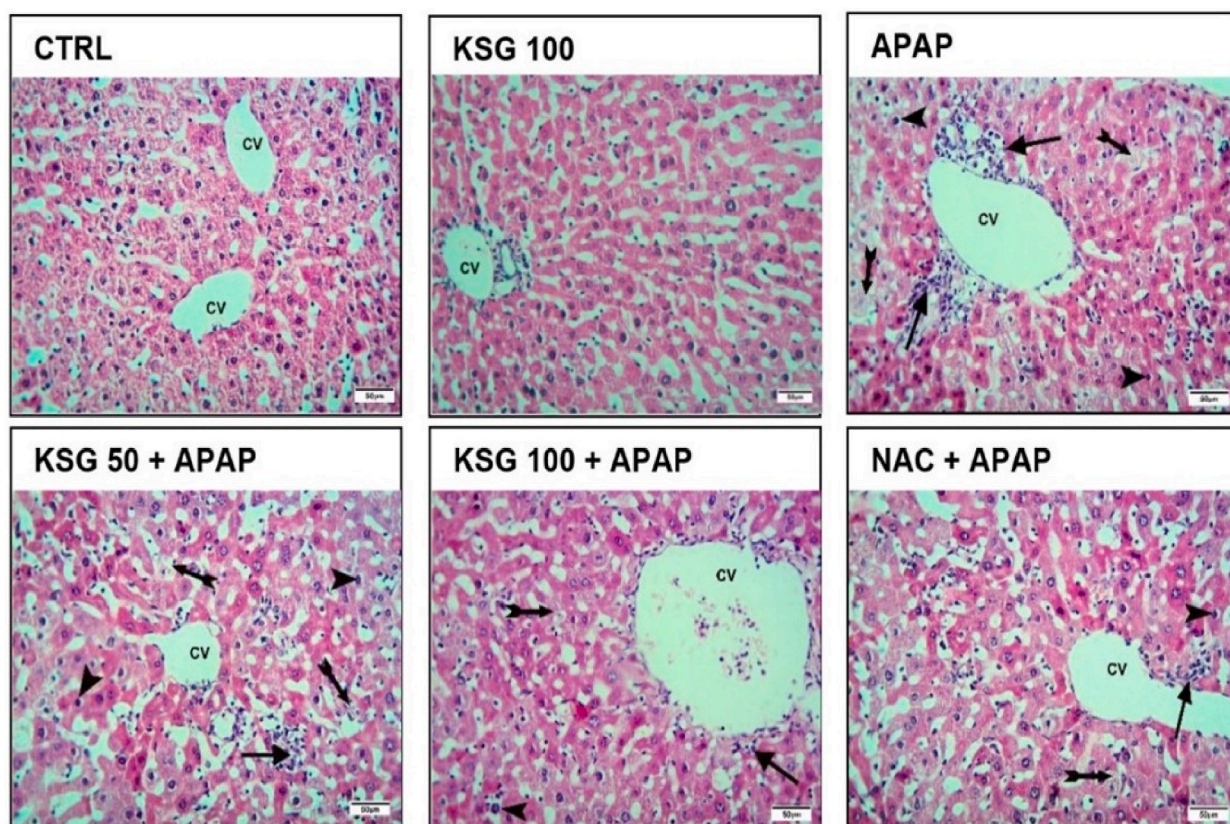
Fig. 1. KSG improved histopathological lesions of APAP-induced ALI in mice.
Liver specimen stained with H&E (× 400): Control and KSG groups exhibited normal liver histology regularly arranged plates of hepatocytes radiating from the central vein (CV); APAP group displayed hepatic lesions in the form of perivascular inflammatory cell infiltration (arrows); many individual hepatocytes with vacuolated cytoplasm (tailed arrows) and pyknotic nuclei (arrowheads); KSG + APAP groups showed remarkable improvement in APAP-induced hepatic lesions; NAC + APAP showed very mild pathological changes.

3. Results

For all the measured biochemical, histological, and molecular parameters, the KSG group exhibited a non-significant difference compared to the control group.

3.1. KSG ameliorated APAP-induced ALI

APAP overdose resulted in a progressive ALI as presented by deteriorated histopathology of the liver as focal hepatic inflammation and necrosis compared to normal histology of the control mice (Fig. 1).

These histopathological results of liver tissue were confirmed by the biochemical results as APAP induced a significant rise in serum levels of AST, ALT, ALP, LDH, and γ-GT when compared to control mice. Administration of KSG significantly reversed all the abovementioned APAP-induced pathological changes that were relatively comparable to NAC effects (Table 1).

3.2. KSG attenuated APAP-induced oxidative stress and boosted the antioxidant status of the hepatic tissue

APAP administration augmented the oxidative burden of the hepatic tissue simultaneously with the withholding of the antioxidants. Markers of oxidative stress, 4-HNE, and MDA were significantly increased in the APAP group. In addition, markers of antioxidant capacity of the hepatic tissue such as GSH, GSH-Px, GST and SOD were relatively depleted in the APAP group (Table 2). KSG successfully hindered APAP-induced lipid peroxidation as it attenuated 4-HNE and MDA compared to the APAP group as well as it significantly intensified GSH, GSH-Px, GST, and SOD compared to the APAP group.

3.3. KSG alleviated APAP-induced inflammatory response in the hepatic tissue

In Fig. 2, APAP overdose resulted in a significant elevation in the levels, as well as the mRNA and protein immuno-expression of the inflammatory cytokines: IL-6 and TNF-α in the hepatic tissues compared to that of the control mice (Fig. 2 A and B). Furthermore, there was a marked decline in the level and mRNA of the anti-inflammatory cytokine IL-10 (Fig. 3A and B). However, KSG pretreatment effectively repressed both, the significant rises of TNF-α and IL-6 and the decline of IL-10.

3.4. KSG opposed APAP-induced activation of NF-κB and enhanced Nrf2 activation in the hepatic tissue

NF-κB signaling is activated following APAP injection as shown through the marked rise in the level, mRNA, and immuno-expression of NF-κB (Fig. 4A). On the other hand, the Nrf2 binding activity, mRNA, and protein immuno-expression were slightly depressed following the APAP challenge (Fig. 4B). KSG pretreatment resulted in a significant reduction in the level, mRNA, and immuno-expression of NF-κB compared to normal mice. Notable enhancement of Nrf2 activity, mRNA, and protein immuno-expression was noticed in KSG + APAP groups (Fig. 4A and B).

3.5. KSG inhibited ASK-1/JNK signaling and attenuated APAP-induced apoptotic response in the hepatic tissue

As presented in Fig. 5A, APAP noticeably increased the level of ASK-1 and JNK. Moreover, APAP induced a significant diminish in the anti-apoptotic marker Bcl2 concurrently with marked elevation in the apoptotic markers; Bax and caspase-3 compared to the control group (Fig. 5B and C). The protein immuno-expression of Bcl2 was lessened and that of caspase-3 was heightened in the APAP group. Contrarily, KSG pretreated groups exhibited the reverse of APAP-induced changes in expression and level of Bcl2, Bax, and caspase-3.

Table 1

KSG reduced serum parameters of APAP-induced ALI in mice.

	CTRL	KSG 100	APAP	KSG 50 + APAP	KSG 100 + APAP	NAC + APAP
ALT (IU/L)	29.33 ± 3.22	30.33 ± 1.8	296 ± 23.25 [c]	224.8 ± 22.36 [c d]	143.8 ± 9.8 [c f]	134 ± 12.48 [c f]
AST (IU/L)	44.5 ± 3.66	39.17 ± 2.98	457.2 ± 45.39 [c]	329 ± 30.6 [c d]	218.7 ± 20.31 [c f]	169.7 ± 14.21 [a f]
ALP (IU/L)	25.5 ± 1.86	25.3 ± 2.1	282.2 ± 4.08 [c]	205.3 ± 13.36 [c f]	137.8 ± 14.76 [c f]	96.17 ± 7.21 [c f]
LDH (IU/L)	173 ± 6.31	187 ± 18.9	820.7 ± 53.89 [c]	611 ± 57.01 [c e]	462.2 ± 33.29 [c f]	389.3 ± 27.67 [b f]
γ-GT (IU/L)	22.67 ± 2.19	24.33 ± 2.63	91.33 ± 8.1 [c]	63.83 ± 5.41 [c e]	51.83 ± 3.1 [b f]	39.67 ± 3.37 [f]

Serum parameters of hepatic injury: Alanine aminotransferase (ALT); Aspartate aminotransferase (AST); Alkaline phosphatase (ALP); Lactate dehydrogenase (LDH); gamma-glutamyl transferase (γ-GT). Data are mean ± SEM (n = 6).

[a] $P < 0.05$.
[b] $P < 0.01$.
[c] $P < 0.001$ vs control group.
[d] $P < 0.05$.
[e] $P < 0.01$.
[f] $P < 0.001$ vs APAP group (one-way ANOVA).

Table 2

KSG attenuated APAP-induced oxidative stress and enhanced antioxidant status of the hepatic tissue.

	CTRL	KSG 100	APAP	KSG 50 + APAP	KSG 100 + APAP	NAC + APAP
4-HNE (µg/ml)	0.76 ± 0.04	0.65 ± 0.06	1.9 ± 0.08[c]	1.3 ± 0.1[b, f]	0.93 ± 0.08[f]	0.82 ± 0.06[f]
MDA (nmol/g tissue)	25.2 ± 1.4	24.1 ± 1.7	78.7 ± 4.4[c]	53.3 ± 3.6[c, f]	44.5 ± 5.1[b, f]	38.3 ± 3.7[f]
GSH (µmol/g tissue)	20.5 ± 1.4	22.2 ± 1.2	7.3 ± 0.9[c]	13.8 ± 1[b, e]	17.7 ± 1.2[f]	19.5 ± 1.1[f]
GSH-Px (U/g tissue)	6.5 ± 0.3	6.8 ± 0.4	3.1 ± 0.3[c]	5.1 ± 0.3[d]	5.7 ± 0.6[e]	5.9 ± 0.5[f]
GST (U/g tissue)	803.7 ± 37.5	830.8 ± 45.1	301.5 ± 32.9[c]	490.2 ± 53.1[c, d]	703.5 ± 27.7[f]	794.8 ± 40.5[f]
SOD (Unit/g tissue)	35.2 ± 2.3	36.5 ± 1.4	17.3 ± 2.2[c]	26.5 ± 1.6[a, d]	28 ± 1.8[e]	29.8 ± 2.2[e]

4-Hydroxynonenal (4-HNE); malondialdehyde (MDA); reduced glutathione (GSH); glutathione peroxidase (GSH-Px); glutathione transferase (GST); superoxide dismutase (SOD). Data are mean ± SEM (n = 6).
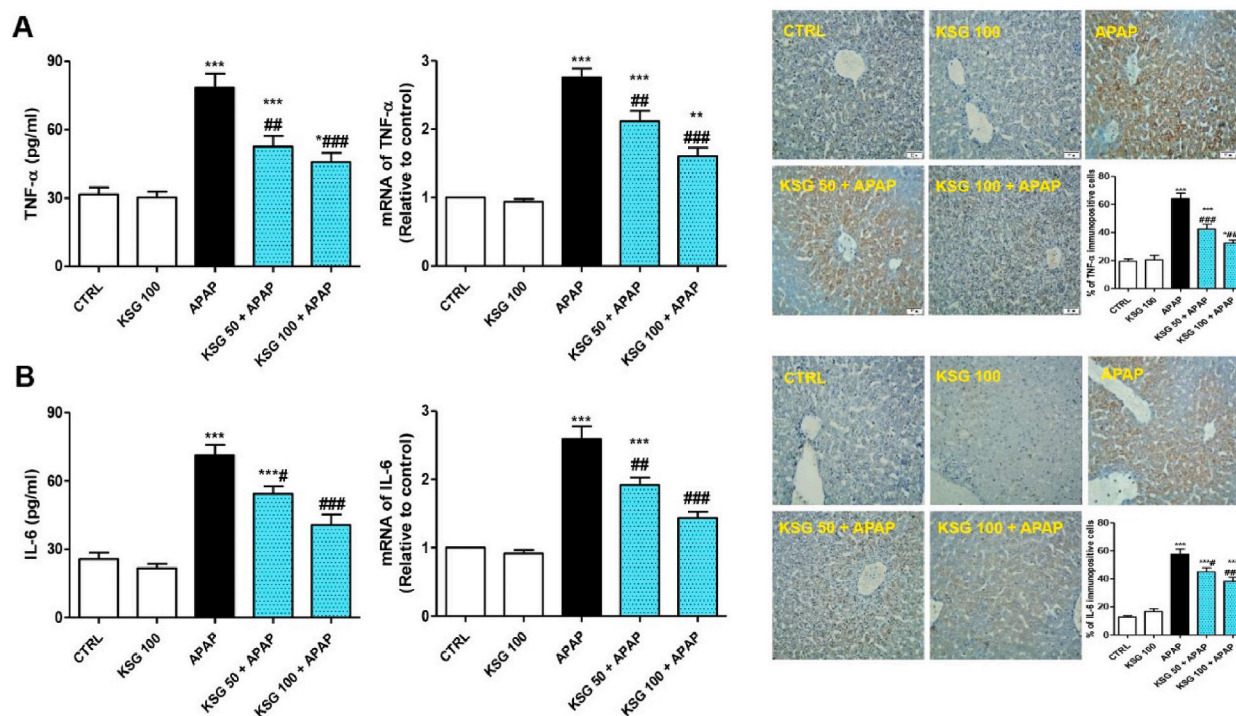
[a] $P < 0.05$.

[b] $P < 0.01$.

[c] $P < 0.001$ vs control group.

[d] $P < 0.05$.

[e] $P < 0.01$.

[f] $P < 0.001$ vs APAP group (one-way ANOVA).

Fig. 2. KSG alleviated APAP-induced inflammatory response in the hepatic tissue.

Level, mRNA and immuno-expression of proinflammatory cytokines: (A) Tumor necrosis factor-α (TNF-α) and (B) Interleukin-6 (IL-6). IHC analysis of TNF-α and IL-6 showed minimal positive stains in the control and KSG 100 groups and high stains in the APAP group for both cytokines. KSG + APAP showed a lower immuno-positive stain. Data are mean ± SEM (n = 6). *$P < 0.05$, **$P < 0.01$, ***$P < 0.001$ vs control group; #$P < 0.05$, ##$P < 0.01$, ###$P < 0.001$ vs APAP group (one-way ANOVA).

3.6. Docking results

The findings of XP docking foretell noteworthy chemical interactions and binding affinities between KSG and the examined proteins i.e., JNK, KEAP1, and ADK1 expressed as docking scores and summarized in Table 3.

It can be spotted from Fig. 6 that KSG projected hydrogen bonds to Ser363, Asn382, and Arg483 as well as water-mediated hydrogen bonds to Ser363 and Arg414 in the KEAP-1 binding site (Fig. 6). In addition, hydrophobic interactions were noticeable with Tyr334, Phe478, Tyr525, Ala556, Tyr572, and Phe577. Whereas π-cation was witnessed with Arg415 and π stacking with Tyr572 residue. On the other hand, KEAP1′s co-crystalized ligand showcased hydrogen bonds to Ser508, Arg415, Ser555, and Gln530. Hydrophobic interactions were observed with Tyr525, Ala556, Tyr572, and Phe577, while π stacking with Tyr525.

The interactions diagram in Fig. 7 highlights hydrogen bonds at Met111, Gly38, water mediated hydrogen bonds at Ile32, Gln117,
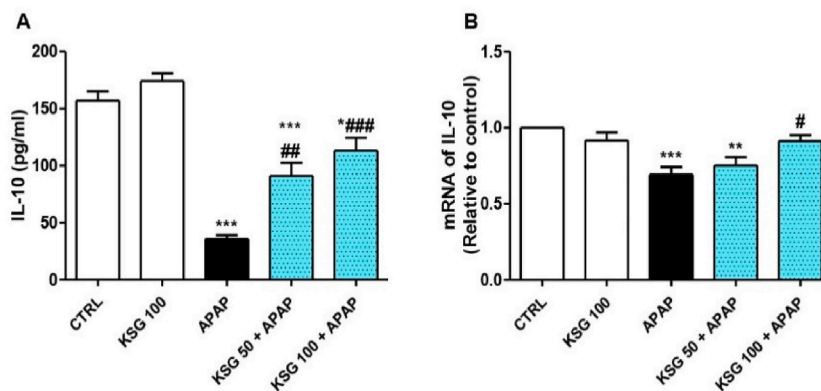
Fig. 3. KSG counteracted APAP-induced decrease in the (A) level and (B) mRNA expression of the anti-inflammatory cytokine, Interleukin-10 (IL-10) in the hepatic tissue.
Data are mean ± SEM (n = 6). *P < 0.05, **P < 0.01, ***P < 0.001 vs control group; #P < 0.05, ##P < 0.01, ###P < 0.001 vs APAP group (one-way ANOVA).
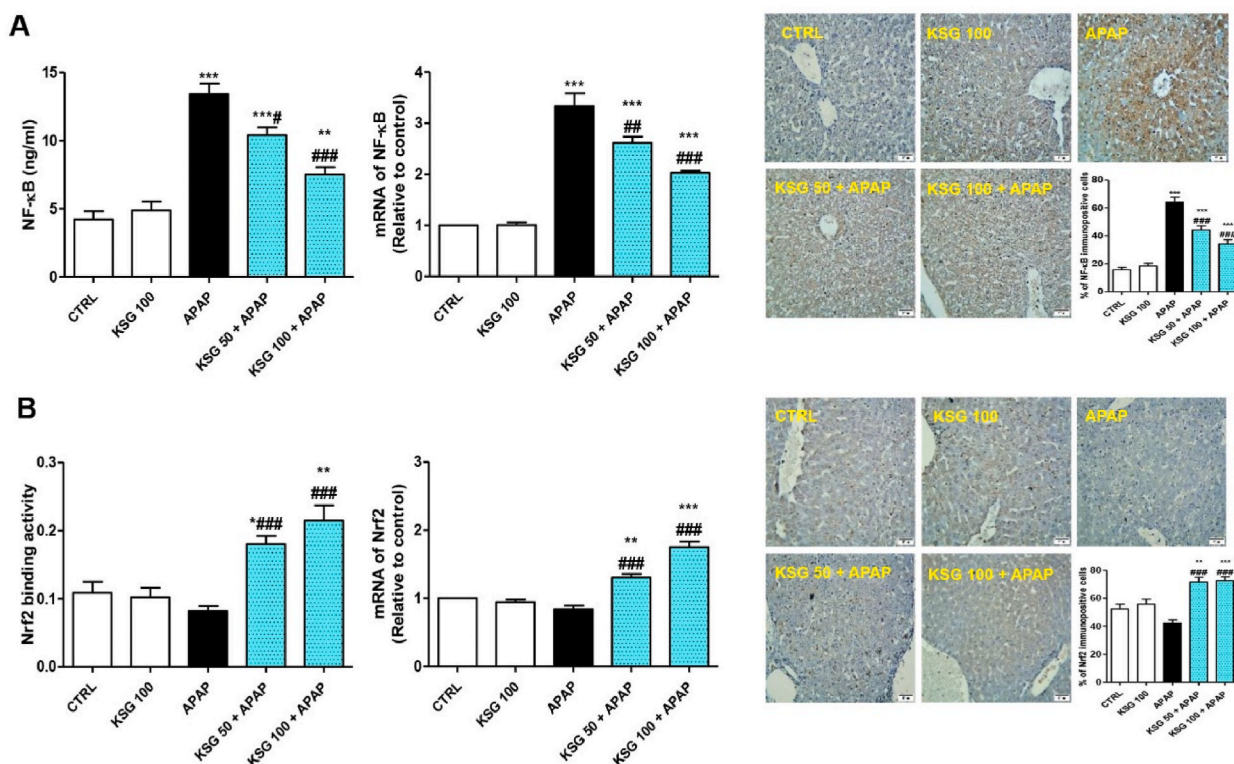

Fig. 4. KSG opposed APAP-induced activation of NF-κB and enhanced Nrf2 activation in the hepatic tissue.
(A) Level, mRNA and immuno-expression of NF-κB. The immuno-stain of NF-κB was deep in a specimen of APAP group while it was attenuated in KSG + APAP groups. (B) The binding activity, mRNA and immuno-expression of Nrf2. The immuno-stain for Nrf2 was enhanced in KSG + APAP groups compared to little stain in APAP group. Data are mean ± SEM (n = 6). *P < 0.05, **P < 0.01, ***P < 0.001 vs control group; #P < 0.05, ##P < 0.01, ###P < 0.001 vs APAP group (one-way ANOVA).

and hydrophobic interactions at Ile32, Val40, Ala53, Leu110, Met111, Val158, and Lue168 in KSG-JNK1(PDB:3PZE) complex (Fig. 7). Meanwhile JNK1- co-crystalized ligand complex projected hydrogen bonds at Glu109, Met111 and hydrophobic interactions at Ile32, Val40, Ala53, Leu110, Met111, Val158, Lue168, Ile86, and Met108 amino acids.

It can be seen from Fig. 8 that KSG has formed hydrogen bonds with chain B at Try814, Asp822, and Val757. It also constructed two water mediated HBs with Lue686 and Lys709. KSG interacted hydrophobically with both chains; chain A at Tyr814 while interacted with chain B at Lue686, Val694, Ala707, Val738, Met754, and Lue810. Conversely, the co-crystalized ligand has built three HB with
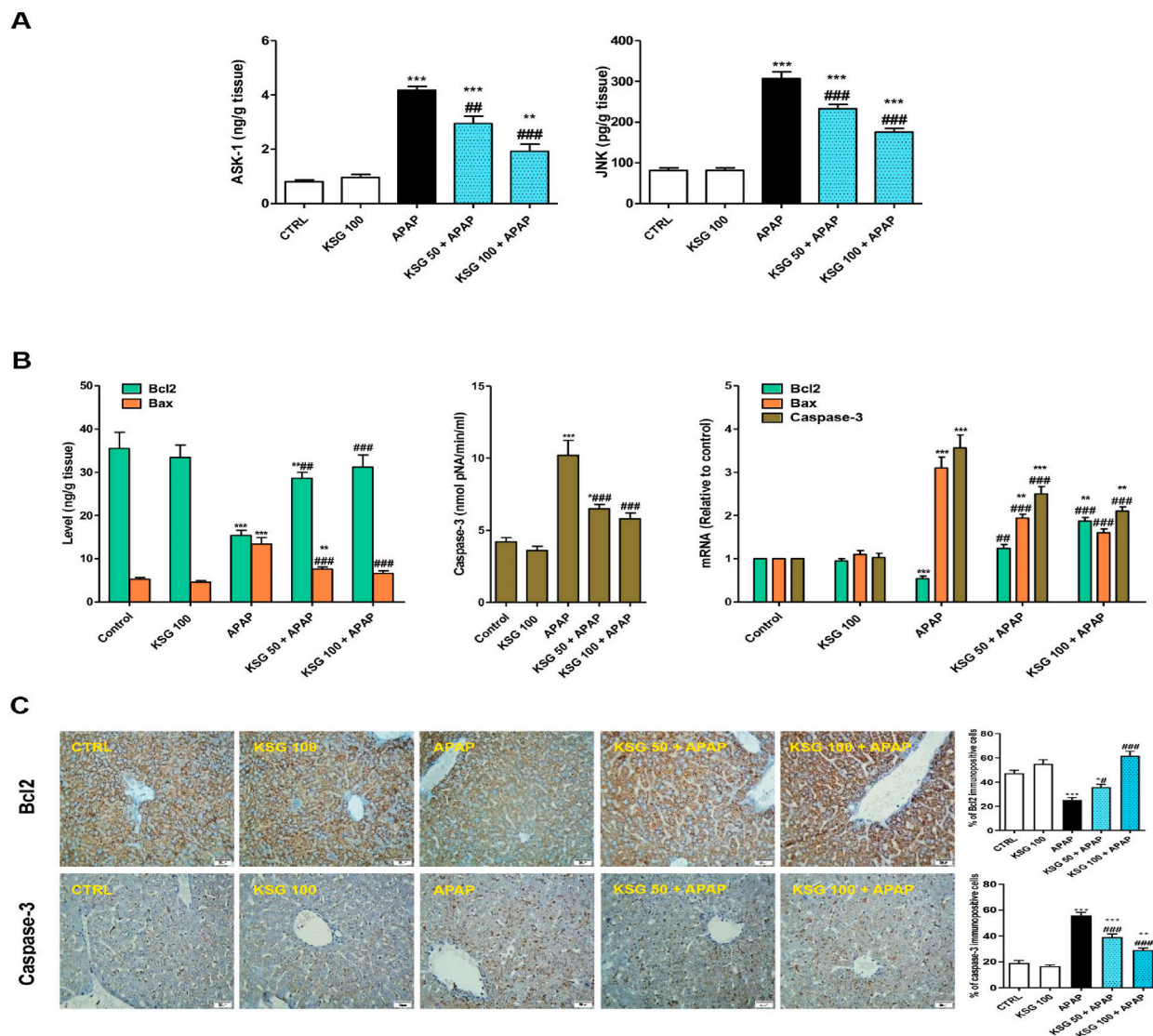
Fig. 5. KSG inhibited ASK-1/JNK signaling and attenuated APAP-induced apoptotic response in the hepatic tissue.
(A) Level of JNK and ASK-1. (B) Level and mRNA of Bcl2, Bax and caspase-3. (C) Immuno-expression of Bcl2 and caspase-3. The immuno-stain of Bcl2 was declined after APAP in contrast to caspase-3 whose immuno-stain was deepened following APAP challenge. These effects were reversed in KSG + APAP groups. Data are mean ± SEM (n = 6). *$P < 0.05$, **$P < 0.01$, ***$P < 0.001$ vs control group; #$P < 0.05$, ##$P < 0.01$, ###$P < 0.001$ vs APAP group (one-way ANOVA).

Lys769, and one with Gly759 amino acids at chain B, whereas hydrophobic interactions were observed with A Tyr814 of chain A, and Gly689, Lue686, Pro758, Lue765, Lue810 of chain B.

3.7. Insilco toxicity studies

Toxicity studies of KSG through the Pro Tox II web server yielded variable results, the most influential parameters have been selected and listed in Table 4. We had chiefly focused on hepatotoxicity, carcinogenicity, immunotoxicity, mutagenicity, and cytotoxicity. Furthermore, we leveraged Pro Tox II to foresee the plausible toxicity class and the lethal dose.

4. Discussion

4.1. Experimental work

APAP overdose-induced ALI is commonly seen in clinical practice, even though diverse therapeutics are missing. Hence, searching

Table 3

The docking scores and the observed bonds for KSG and the co-crystalized ligand (reference) for each protein. (wm: water-mediated, π-ca: π-cation, π-st: π stacking).

Title	docking score	XP GScore	H-Bonds	Hydrophobic	Others
KEAP1 (PDB ID: 7OFE)					
KSG	−7.525	−7.561	Ser363, Asn382, Arg483, Ser363 (wm), Arg414 (wm)	Tyr334, Phe478, Tyr525, Ala556, Tyr572, Phe577	Arg415(π-ca), Tyr572 (π-st)
Reference	−6.633	−6.633	Ser508, Arg415, Ser555, Gln530	Tyr525, Ala556, Tyr572, Phe577	Tyr525 (π-st)
JNK1 (PDB:3PZE)					
KSG	−12.301	−12.337	Met111, Gly38, ILE32 (wm), Gln117 (wm), Lys 55	Ile32, Val40, Ala53, Leu110, Met111, Val158, Lue168	–
Reference	−8.028	−8.028	Glu109, Met111	Ile32, Val40, Ala53, Leu110, Met111, Val158, Lue168, ILE86, Met108	–
ASK1 (PDB ID: 6E2N)					
Reference	−9.746	−9.746	B Lue686 (wm), B Lys709 (wm), B Try814, B Asp822, B Val757	A Tyr814, B Lue686, B Val694, B Ala707, B Val738, B MET754, B Lue810	–
KSG	−8.926	−8.962	B Lys769 (3HB), B Gly759, B Val757	A Tyr814, B Gly689, B Lue686, B Pro758, B Lue765, B Lue810	–
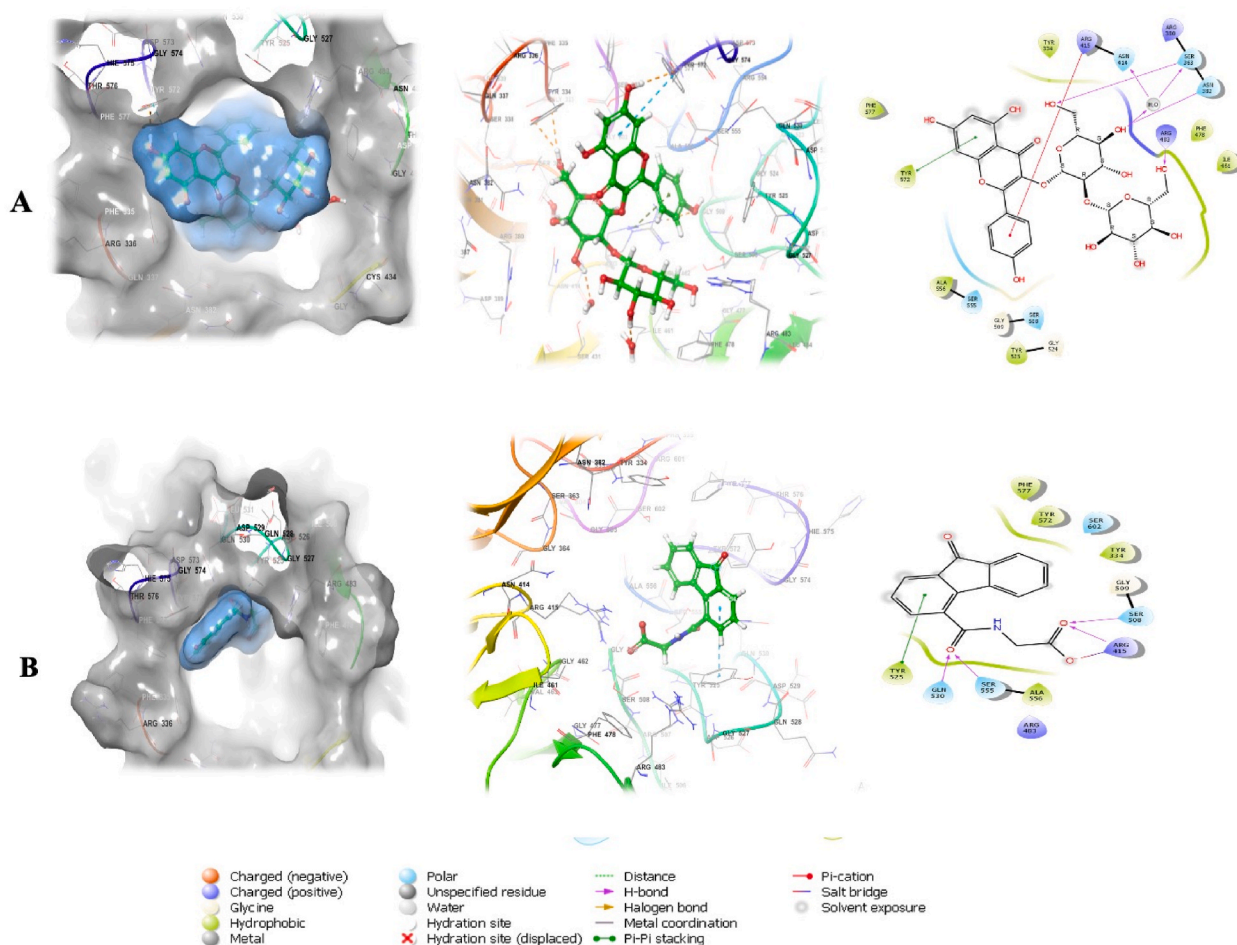
Fig. 6. The 2D and 3D interactions between (A) KSG and (B) the co-crystalized reference with KEAP-1 (PDB ID: 7OFE) predicted by XP docking of Schrodinger's Maestro 12.8. The colored legends indicate the name and the type of interaction.

for new effective candidates is necessary. The pathogenesis of APAP is mainly attributed to excessive oxidative stress, inflammation, and apoptosis [13]. So, agents that could inhibit these pathogenic players might be a potentially effective strategy for APAP intoxication. The present study is the first to report that the new kaempferol derivative, KSG can protects hepatocytes against APAP-induced ALI. The hepatoprotective activity of KSG is mainly associated with the inhibition of NF-κB/TNF-α/ILs, up-regulation of Nrf2/Bcl2, and
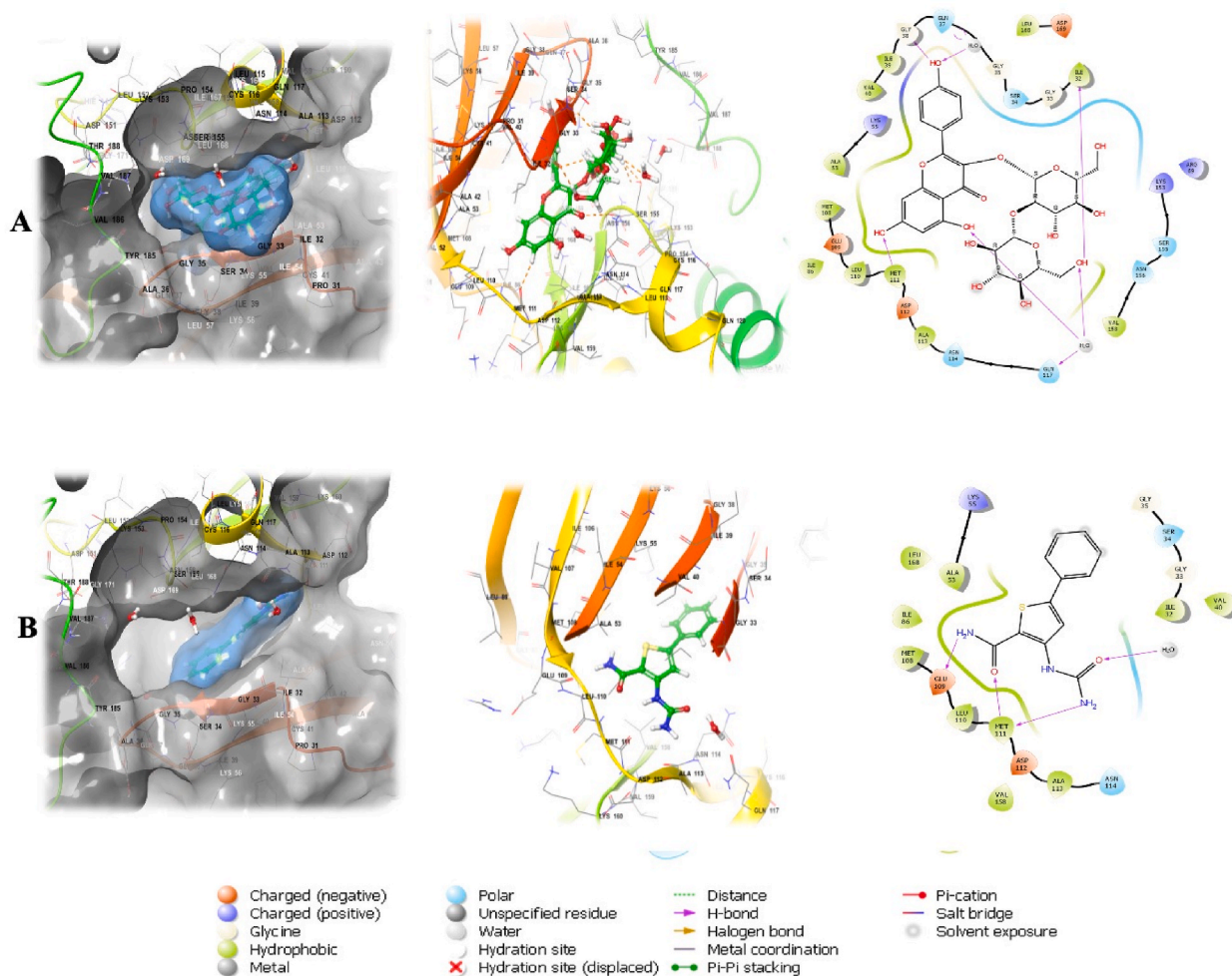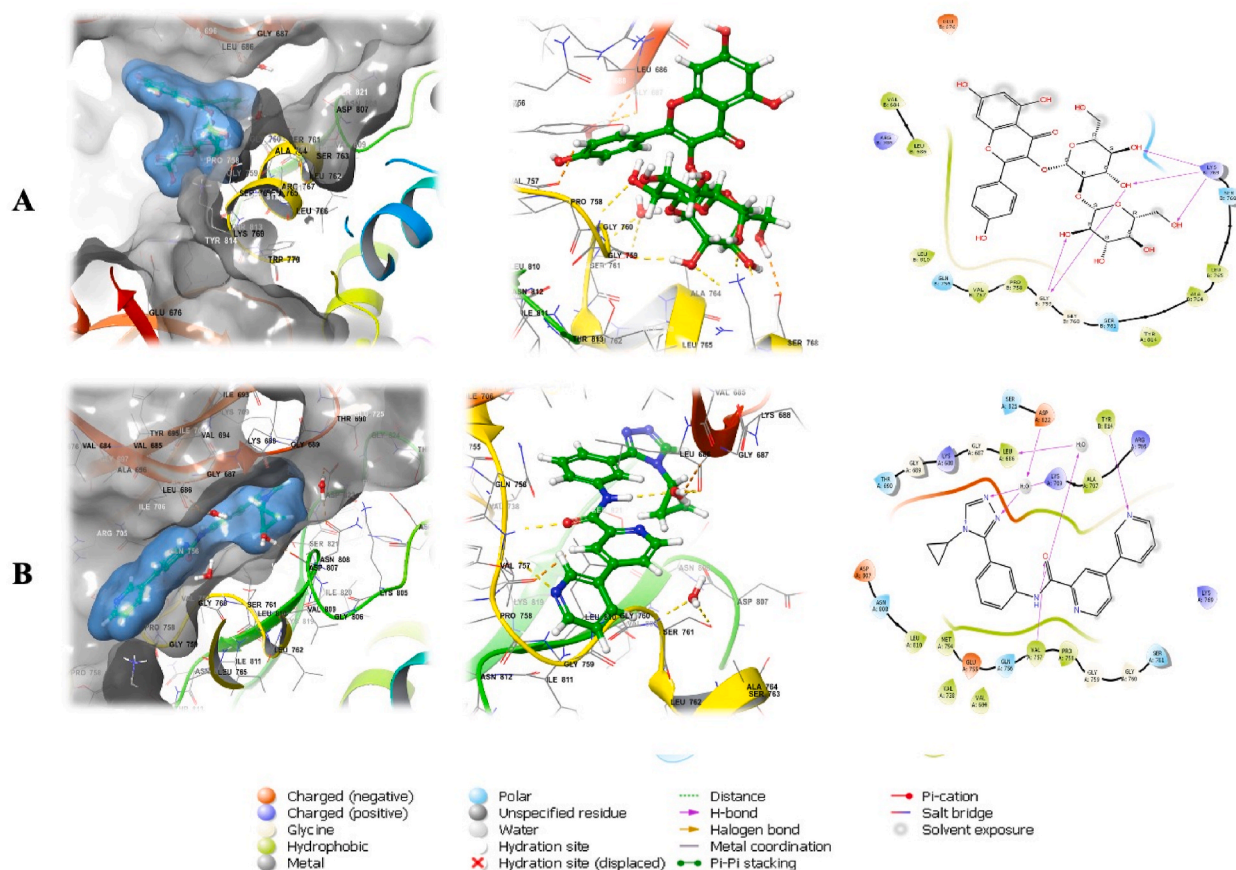
Fig. 7. The 2D and 3D interactions between (A) KSG and (B) the co-crystalized reference with JNK (PDB ID: 3PZE) predicted by XP docking of Schrodinger's Maestro 12.8. The colored legends indicate the name and the type of interaction.

suppression of ASK-1/JNK/Bax/caspase-3 (Fig. 9).

Based on the histopathology and test results, animals subjected to APAP overdose exhibited substantial pathological hepatic lesions and a notable elevation in serum parameters of hepatic damage (ALT, AST, ALP, LDH, and γ-GT). These observations come along with the data of earlier studies that documented the significant hepatotoxic actions of APAP [17,54,55]. Interestingly, pretreatment with KSG significantly alleviated the pathological lesions and reduced the elevated levels of transaminases, ALP, LDH, and γ-GT, indicating protection of the liver's integrity and function by KSG. Importantly, the hepatoprotective activity of different derivatives of kaempferol against experimental hepatic injury has been shown previously [30,31,56,57].

Oxidative stress is considered a cornerstone in the progression of APAP-induced hepatic damage. The highly reactive metabolite of APAP: NAPQI mediates the toxicity of APAP through the depletion of cellular GSH, binding to cellular proteins, excessive ROS formation, and generation of a state of oxidative stress-induced ALI [14,58,59]. In line with these previous reports, our study revealed the disrupted oxidant/antioxidant hemostasis following the injection of a high dose of APAP. That was evident through the elevation of lipid peroxidative parameters; 4-HNE and MDA. The restricted antioxidant capacity of the liver was obvious through the remarkable reduction in GSH, GSH-Px, GST, and SOD activity. Pretreatment with KSG suppressed APAP-mediated oxidative damage in the hepatic tissue contaminant with enhanced antioxidant capacity suggesting that KSG has marked free radical scavenging properties that helped to protect the oxidant/antioxidant balance and hence safeguarded the liver against APAP-induced damage. These data are in line with previous studies that clarified the antioxidant potential of kaempferol derivatives [30,31,56,57].

Oxidative stress and inflammation crosstalk mediate the pathogenic pathways of APAP-induced liver damage. Oxidative stress exacerbates hepatic damage through activation of multiple inflammatory transcription factors which triggers the overexpression of pro-inflammatory proteins that aggravate inflammation [3,60]. Our data confirmed the elevation of the level and expression of inflammatory cytokines, TNF-α and IL-6, following APAP injection while there was a marked reduction in the level and expression of IL-10, an anti-inflammatory cytokine. These results came in line with former studies that revealed the overexpression and excessive

Fig. 8. The 2D and 3D interactions between (A) KSG and (B) the co-crystalized reference with ASK1 (PDB ID: 6E2N) predicted by XP docking of Schrodinger's Maestro 12.8. The colored legends indicate the name and the type of interaction.

release of TNF-α and IL-6 in the hepatic tissue of the APAP group [60,61]. KSG pre-treatment counteracted the rise of inflammatory cytokines which limited the inflammatory response following APAP injection. It may be acceptable to say that KSG has substantial anti-oxidative and anti-inflammatory activities.

Among the inflammatory pathways that control the inflammatory response during APAP-mediated hepatotoxicity is NF-κB, a nuclear transcription factor, that is the most often reported. NF-κB becomes activated in response to many stimuli as excessive ROS, to be released and translocated into the nucleus where it induces the overexpression of inflammatory cytokines such as TNF-α and IL-6. Our data confirmed the activation of NF-κB after APAP challenge which agrees with previous work findings [4,10,61,62]. KSG pre-treatment showed a remarkable inhibition of NF-κB activation, which may be responsible in part for its anti-inflammatory activity. These data are consistent with previous studies which showed the ability of kaempferol to inhibit the activation of NF-κB [31,63,64]. The activation of NF-κB has been shown to impact an important antioxidant stress modulator which is Nrf2 signaling. Nrf2 regulates the inducible and constitutive expression of numerous genes involved in antioxidative defence and drug detoxification. The nuclear factor Nrf2 plays a key role in resisting APAP-induced liver injury as it induces the expression and release of many antioxidant mediators that effectively can oppose the progress of the hepatic damage. Elevation of Nrf2 expression showed a protective effect on the liver against APAP-induced ALI [13,55,59]. In this study, KSG treatment enhanced Nrf2 mRNA expression and its binding activity, suggesting that Nrf2 activation is one of the main mechanisms involved in the beneficial effect of KSG. Our results are confirmed by the data of earlier reports which demonstrated the ability of kaempferol to enhance the expression of Nrf2 in liver tissue intoxicated by carbon tetrachloride [63], acetaminophen [56], or cadmium chloride [64].

The critical role of JNK in APAP-induced cell death in mice has been documented [65,66]. Importantly, after the translocation of p-JNK to the mitochondria [12], p-JNK enhances mitochondrial oxidant stress which results in JNK-dependent cell death in APAP-induced hepatotoxicity [67,68]. Noteworthy, JNK is not a redox-sensitive kinase. JNK is regulated by other upstream kinases including ASK-1 [11] which is activated in response to oxidative and inflammatory stimuli such as ROS or cytokines. Previous reports demonstrated inhibition of ASK1 inhibitor [65] or JNK phosphorylation [2,68] significantly attenuated APAP hepatotoxicity. Our data indicated that APAP injection markedly elevated the levels of hepatic ASK-1 and JNK. This was significantly attenuated by pre-treatment with KSG. Therefore, it may be acceptable to presume that KSG hepatoprotective activity is mediated through suppressing the ASK-1/JNK pathway. It is worth to mention that kaempferol derivatives modulated MAPK pathways in case of experimental

Table 4
The anticipated toxicity parameters for KSG.

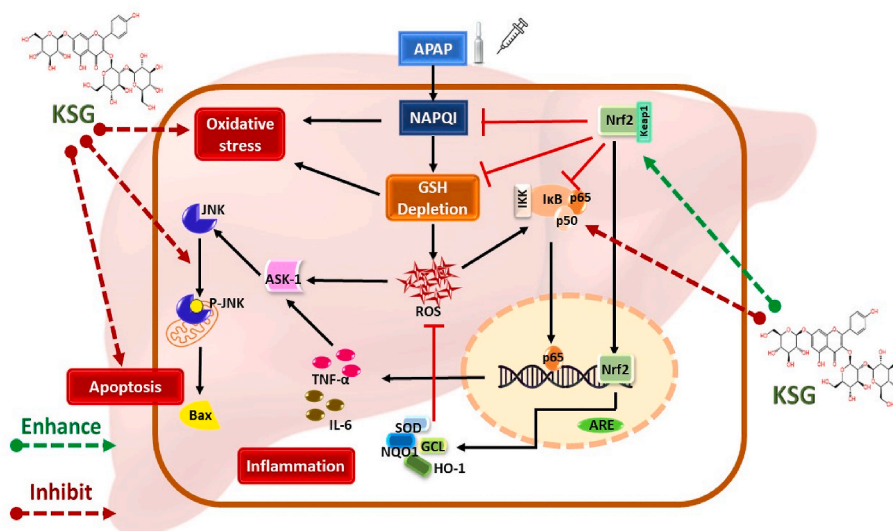| LD50 (mo/kg)	Toxicity Class	Hepatotoxicity		Carcinogenicity		Immunotoxicity		Mutagenicity		Cytotoxicity	
5000	5	Prediction Inactive	Probability 0.83	Prediction Inactive	Probability 0.85	Prediction Active	Probability 0.89	Prediction Inactive	Probability 0.74	Prediction Inactive	Probability 0.67

Fig. 9. A schematic illustration of the main mechanisms that mediate the beneficial activity of KSG against APAP-induced ALI.

hepatic failure [69]. ASK-1/JNK activation has been linked to the induction of apoptotic changes as activation of Bax, increases mitochondrial permeability and cytochrome C release with subsequent activation of caspases such as caspase-3 [70,71]. Hence, the involvement of apoptosis in the pathogenic events of APAP-induced ALI is confirmed. Previous studies have shown the disruption between the pro-apoptotic and anti-apoptotic mediators as APAP overdose increases the expression of Bax as well as caspase-3 activity with diminished Bcl-2 expression [72,73]. Consistent with these reports our data showed that APAP overdose resulted in an elevation in the mRNA and level of Bax and caspase 3, as well as a decline of Bcl2 level. However, these changes were significantly lowered in response to KSG pretreatment, suggesting that the hepatoprotective activity of KSG may be due to suppression of apoptosis. These data are in harmony with previous reports that demonstrated the anti-apoptotic activities of kaempferol [30].

4.2. Computational work

Extra-precision GLIDE docking is a coherent strategy in which the ligand sampling and the applied scoring procedure were optimized simultaneously which gave it a prestigious simulation power. This progress was driven by the scarcity of reliable pose prediction techniques and quantitative ranking for the corresponding binding affinities for these poses. The previous literature had interestingly displayed that GLIDE XP docking does not only offer robust energy calculations, but it can reproduce the experimental Ligand-Receptor interaction as well. Kelch-like ECH-associated protein 1 (Keap1) is condemned to be a part of the pathology of numerous diseases and inflammatory responses [74,75]. Herein, the results of Kaempferol-3-sophoroside-7-glucoside docking against Keap1 protein have shown prosperous findings. It can be seen from Table 3 that KSG owed superior binding affinity in comparison with the co-crystalized potent Keap1 inhibitors (reference), this superiority is reflected in the docking score of **-7.525** kcal/mol for KSG versus **-6.633** kcal/mol for the reference. Relevant literature reports have linked hydrogen bond formation with Keap1′s protein-protein interaction domain (Arg415, Arg483, Ser508, Ser363, Arg380, and Asn382) with high ligand binding affinity [75]. The retrospection of the depicted interactions in Fig. 7 in light of these conclusions explain the superiority of KSG in the estimations of binding affinity since it formed hydrogen bonds at Ser363, Asn382, Arg483, and Ser363 (wm) in addition to π-cation at Arg415 (Fig. 7). Meanwhile, the reference molecule constructed hydrogen bonds at Ser508, Arg415, and Gln530 in Keap1′s interacting domain. Studies also showed that π stacking with Tyr572 is a shared feature among Keap1 inhibitors [75,76], which was noticeable at the phenolic ring in kaempferol-3-sophoroside-7-glucoside but was absent in the co-crystalized ligand-Keap1 interaction. Both compounds presented massive hydrophobic interaction with the Keap1 binding domain though KSG outweighed the co-crystalized ligand in this respect. These findings suggested that kaempferol-3-sophoroside-7-glucoside carries a distinctive potential for Keap1 inhibition.

c-Jun NH2-terminal kinase 1 (JNK1) is one of the stress kinases that interact with specific pathways to contribute to lots of physiological and pathophysiological conditions including ALI [77,78]. For decades, the discovery of selective JNK inhibitors was challenged by the structural similarity between JNKs isoforms and between the JNKs family and the other kinases i.e., ERK2, P38, CHKs, CDKs, etc [79].

Surprisingly, KSG showed a high docking score value of **-12.301** kcal/mol in comparison with **-8.028** kcal/mol for thiophene carboxamide urea (reference). Moreover, KSG presented plenty of interactions that are renowned prerequisites for JNK1 selective inhibition. This imposes hydrogen bonding at the hinge residue Met111 (fingerprint for selective JNK1 inhibitors) and Lys 55, hydrophobic interaction at ILE32, and hydrophobic interaction near the gatekeeper at Leu110 and Met111 (Fig. 8). These interactions are directly correlated JNK1 inhibitors with selectivity and potency [80–82]. Collectively, these observations nominate KSG as a potential JNK1 selective inhibitor.

Apoptosis signal–regulating kinase 1 (ASK1) is an abundant member of the mitogen-activated protein kinase, it cooperated with ubiquitous pathways to control oxidative stress. Phosphorylation of ASK1′s Thr845 in the activation loop boosts ASK1′s catalytic potential. The phosphorylated ASK1 activates MAPKKs which subsequently activates MAPKs, p38, and c-Jun N-terminal kinase (JNK) [83]. In this study, we had inversely docked ASK's potent inhibitor GS-444217 ($K D = 4.1$ nM) to be used as a reference. It is noteworthy that the docking process had completely reproduced the documented interactions for ASK1 inhibition. Henceforth, hydrogen bond was noticed at the hinge residue Val757, Lys709, and cross-dimer hydrogen bond to Tyr814 which is renowned as peculiar and related to the higher potency. the *N*-cyclopropyl group of the triazole occupies the groove made by residues Ser821, Asp822, Leu810, and Asn808 [83]. Although KSG presented comparable binding affinity (−**8.926** kcal/mol vs **-9.746** kcal/mol), it showcased different interaction patterns, four hydrogen bonds were observed at the hinge region at Lys769 and Gly759, and Val757 (Fig. 8) which were stated to be preferential for ASK1 inhibition. KSG did not fill the formerly mentioned pocket, it only contacted it hydrophobically at LUE810. Taking these notes, Kaempferol-3-sophoroside-7-glucoside conveys a considerable likelihood for ASK1 inhibition.

Recalling the data in Table 4, Pro Tox-II categorizes oral toxicity based on the median lethal dose (LD$_{50}$) expressed in milligrams per kilogram of body weight. An LD5$_0$ dose of 5000 mg/kg positions Kaempferol-3-sophoroside-7-glucoside at category 5 (slightly toxic). The results refer to an existent risk of immunotoxicity, nevertheless, no risk of hepatotoxicity, carcinogenicity, mutagenicity, or cytotoxicity.

5. Conclusions

In summary, KSG counteracted APAP-associated oxidative stress, inflammatory response, and apoptotic events in the hepatic tissue via modulation of NF-κB/Nrf2 and ASK-1/JNK/caspase-3 signaling. Computational analysis of KSG versus the intrinsic regulators in ALI demonstrated discernible interaction energies. However, the interactions of KSG with JNK1 and Keap1 endorsed its potential to selectively interact with these kinases. Meanwhile, KSG's selectivity towards ASK1 might be questionable. We recommend further investigations to comprehend the beneficial role of KSG against inflammatory hepatic dysfunction more vividly.

Ethics declaration

The Research Ethical Committee of the Faculty of Pharmacy, King Abdulaziz University certified the study protocol (number PH-115-40) that follows the NIH Guides for experimental animals' care and use.

Funding

Ethical approval

The study protocol was approved by the Research Ethical Committee of Faculty of Pharmacy, King Abdulaziz University under the number PH-115-40.

Data availability statement

All data required to support this study is already mentioned in the manuscript and Supplementary Materials.

CRediT authorship contribution statement

Gamal A. Mohamed: Writing – review & editing, Resources, Project administration, Funding acquisition, Formal analysis, Data curation, Conceptualization. **Dina S. El-Agamy:** Writing – review & editing, Writing – original draft, Validation, Methodology, Formal analysis, Data curation, Conceptualization. **Hossam M. Abdallah:** Writing – review & editing, Validation, Formal analysis, Data curation. **Ikhlas A. Sindi:** Writing – review & editing, Resources, Formal analysis, Data curation. **Mohammed A. Almogaddam:** Writing – review & editing, Writing – original draft, Software, Methodology, Data curation. **Abdulrahim A. Alzain:** Writing – review & editing, Writing – original draft, Validation, Software, Methodology, Conceptualization. **Yusra Saleh Andijani:** Writing – review & editing, Validation, Resources, Formal analysis, Data curation. **Sabrin R.M. Ibrahim:** Writing – review & editing, Writing – original draft, Methodology, Data curation, Conceptualization.

Declaration of competing interest

The authors declare that they have no known competing financial interests or personal relationships that could have appeared to influence the work reported in this paper.

Acknowledgments

Appendix A. Supplementary data

Supplementary data to this article can be found online at https://doi.org/10.1016/j.heliyon.2024.e31448.

List of abbreviations

APAP	Acetaminophen
ALI	APAP-induced acute liver injury
ALT	Alanine transaminase
ALP	Alkaline phosphatase
ASK1	Apoptosis signal-regulating kinase 1
AST	aspartate aminotransferase
Bax	Bcl2-associated X protein
CMC	Carboxymethyl cellulose
DAB	Diaminobenzidine
ELISA	Enzyme-linked immunosorbent assay
GAPDH	Glyceraldehyde-3-phosphate dehydrogenase
GSH	glutathione
GSH-px	glutathione peroxidase
GST	glutathione-s-transferase
γ-GT	gamma-glutamyl transferase
H&E	hematoxylin-eosin
4-HNE	4-Hydroxynonenal
IHC	immunohistochemical
IL	interleukin
JNK	JNK1 (c-Jun N-terminal protein kinase 1)
Keap1	Kelch-like ECH-associated protein 1
LDH	lactate dehydrogenase
MDA	malondialdehyde
NAC	N-acetylcysteine
NAPQI	N-acetyl-p-benzoquinoneimine
NF-κB	nuclear factor kappa B
NLRP3	Nucleotide-binding domain, leucine-rich–containing family, pyrin domain–containing-3
PBS	phosphate-buffered saline
SOD	superoxide dismutase
ROS	reactive oxygen species
TNF-α	tumour necrosis factor-α

References

[1] H. Jaeschke, J.Y. Akakpo, D.S. Umbaugh, A. Ramachandran, Novel therapeutic approaches against acetaminophen-induced liver injury and acute liver failure, Toxicol. Sci. 174 (2020) 159–167.

[2] X. Deng, Y. Li, X. Li, Z. Zhang, S. Dai, H. Wu, F. Zhang, Q. Hu, Y. Chen, J. Zeng, Paeoniflorin protects against acetaminophen-induced liver injury in mice via JNK signaling pathway, Molecules 27 (2022) 8534.

[3] Y. Wang, X. Geng, M. Wang, H. Wang, C. Zhang, X. He, S. Liang, D. Xu, X. Chen, Vitamin D deficiency exacerbates hepatic oxidative stress and inflammation during acetaminophen-induced acute liver injury in mice, Int. Immunopharm. 97 (2021) 107716.

[4] H. Ni, A. Bockus, N. Boggess, H. Jaeschke, W. Ding, Activation of autophagy protects against acetaminophen-induced hepatotoxicity, Hepatology 55 (2012) 222–232.

[5] B.L. Woolbright, H. Jaeschke, Role of the inflammasome in acetaminophen-induced liver injury and acute liver failure, J. Hepatol. 66 (2017) 836–848.

[6] F. Yang, R. Cui, Z. Li, X. Zhang, Y. Jia, X. Zhang, J. Shi, K. Qu, C. Liu, J. Zhang, Methane alleviates acetaminophen-induced liver injury by inhibiting inflammation, oxidative stress, endoplasmic reticulum stress, and apoptosis through the Nrf2/HO-1/NQO1 signaling pathway, Oxid. Med. Cell. Longev. 2019 (2019), 2019.

[7] S. Bhatt, A. Sharma, A. Dogra, P. Sharma, A. Kumar, P. Kotwal, S. Bag, P. Misra, G. Singh, A. Kumar, Glabridin attenuates paracetamol-induced liver injury in mice via CYP2E1-mediated inhibition of oxidative stress, Drug Chem. Toxicol. 45 (2022) 2352–2360.

[8] Z. Du, Z. Ma, S. Lai, Q. Ding, Z. Hu, W. Yang, Q. Qian, L. Zhu, X. Dou, S. Li, Atractylenolide I ameliorates acetaminophen-induced acute liver injury via the TLR4/MAPKs/NF-κB signaling pathways, Front. Pharmacol. 13 (2022) 797499.

[9] F. Liu, H. Lee, C. Liao, A. Chou, H. Yu, Role of NADPH oxidase-derived ROS-mediated IL-6/STAT3 and MAPK/NF-κB signaling pathways in protective effect of corilagin against acetaminophen-induced liver injury in mice, Biology 12 (2023) 334.

[10] R. Yang, C. Song, J. Chen, L. Zhou, X. Jiang, X. Cao, Y. Sun, Q.I. Zhang, Limonin ameliorates acetaminophen-induced hepatotoxicity by activating Nrf2 antioxidative pathway and inhibiting NF-κB inflammatory response via upregulating Sirt1, Phytomedicine 69 (2020) 153211.

[11] H. Nakagawa, S. Maeda, Y. Hikiba, T. Ohmae, W. Shibata, A. Yanai, K. Sakamoto, K. Ogura, T. Noguchi, M. Karin, Deletion of apoptosis signal-regulating kinase 1 attenuates acetaminophen-induced liver injury by inhibiting c-Jun N-terminal kinase activation, Gastroenterology 135 (2008) 1311–1321.

[12] N. Hanawa, M. Shinohara, B. Saberi, W.A. Gaarde, D. Han, N. Kaplowitz, Role of JNK translocation to mitochondria leading to inhibition of mitochondria bioenergetics in acetaminophen-induced liver injury, J. Biol. Chem. 283 (2008) 13565–13577.

[13] Z. Gao, H. Zhan, W. Zong, M. Sun, L. Linghu, G. Wang, F. Meng, M. Chen, Salidroside alleviates acetaminophen-induced hepatotoxicity via Sirt1-mediated activation of Akt/Nrf2 pathway and suppression of NF-κB/NLRP3 inflammasome axis, Life Sci. 327 (2023) 121793.

[14] S.R.M. Ibrahim, D.S. El-Agamy, H.M. Abdallah, N. Ahmed, M.A. Elkablawy, G.A. Mohamed, Protective activity of tovophyllin A, a xanthone isolated from *Garcinia mangostana* pericarps, against acetaminophen-induced liver damage: role of Nrf2 activation, Food Funct. 9 (2018) 3291–3300.

[15] H. Okawa, H. Motohashi, A. Kobayashi, H. Aburatani, T.W. Kensler, M. Yamamoto, Hepatocyte-specific deletion of the keap1 gene activates Nrf2 and confers potent resistance against acute drug toxicity, Biochem. Biophys. Res. Commun. 339 (2006) 79–88.

[16] Z. Gao, W. Yi, J. Tang, Y. Sun, J. Huang, T. Lan, X. Dai, S. Xu, Z. Jin, X. Wu, Urolithin A protects against acetaminophen-induced liver injury in mice via sustained activation of Nrf2, Int. J. Biol. Sci. 18 (2022) 2146.

[17] H. Lv, C. Zhu, W. Wei, X. Lv, Q. Yu, X. Deng, X. Ci, Enhanced Keap1-Nrf2/Trx-1 axis by daphnetin protects against oxidative stress-driven hepatotoxicity via inhibiting ASK1/JNK and Txnip/NLRP3 inflammasome activation, Phytomedicine 1 (2020) 153241, 2020.

[18] P. Tugume, C. Nyakoojo, Ethno-pharmacological survey of herbal remedies used in the treatment of paediatric diseases in Buhunga parish, Rukungiri District, Uganda, BMC Compl. Alternative Med. 19 (2019) 1–10.

[19] M. Ekor, The growing use of herbal medicines: issues relating to adverse reactions and challenges in monitoring safety, Front. Pharmacol. 4 (2014) 177.

[20] A.C. Akinmoladun, K.O. Oguntunde, L.O. Owolabi, O.B. Ilesanmi, J.O. Ogundele, M.T. Olaleye, A.A. Akindahunsi, Reversal of acetaminophen-generated oxidative stress and concomitant hepatotoxicity by a phytopharmaceutical product, Food Sci. Hum. Wellness 6 (2017) 20–27.

[21] B.H. AlSaadi, S.H. AlHarbi, S.R. Ibrahim, A.A. El-Kholy, D.S. El-Agamy, G.A. Mohamed, Hepatoprotective activity of *Costus speciosus* (Koen. Ex. Retz.) against paracetamol induced liver injury in mice, Afr. J. Tradit., Complementary Altern. Med. 15 (2018) 35–41.

[22] M.T. Khayat, K.A. Mohammad, G.A. Mohamed, D.S. El-Agamy, W.M. Elsaed, S.R. Ibrahim, γ-Mangostin abrogates AINT-induced cholestatic liver injury: impact on Nrf2/NF-κB/NLRP3/Caspase-1/IL-1β/GSDMD signalling, Life Sci. 322 (2023) 121663.

[23] S.R. Ibrahim, A. Sirwi, B.G. Eid, S.G. Mohamed, G.A. Mohamed, Summary of natural products ameliorate concanavalin a-induced liver injury: structures, sources, pharmacological effects, and mechanisms of action, Plants 10 (2021) 228.

[24] A.N. Panche, A.D. Diwan, S.R. Chandra, Flavonoids: an overview, J. Nutr. Sci. 5 (2016) e47.

[25] A. Mazumder, A. Sharma, M.A. Azad, A Comprehensive review of the pharmacologicalimportance of dietary flavonoids as hepatoprotective agents, Evid Based Complementary Altern Med. 2023 (2023).

[26] A. Ullah, S. Munir, S.L. Badshah, N. Khan, L. Ghani, B.G. Poulson, A. Emwas, M. Jaremko, Important flavonoids and their role as a therapeutic agent, Molecules 25 (2020) 5243.

[27] A.M. Sayed, E.H. Hassanein, S.H. Salem, O.E. Hussein, A.M. Mahmoud, Flavonoids-mediated SIRT1 signaling activation in hepatic disorders, Life Sci. 259 (2020) 118173.

[28] Q. Yang, L. He, X. Zhou, Y. Zhao, J. Shen, P. Xu, S. Ni, Kaempferol pretreatment modulates systemic inflammation and oxidative stress following hemorrhagic shock in mice, Chin. Med. 10 (2015) 1–7.

[29] J. Ren, Y. Lu, Y. Qian, B. Chen, T. Wu, G. Ji, Recent progress regarding kaempferol for the treatment of various diseases, Exp. Ther. Med. 18 (2019) 2759–2776, 2019.

[30] M. Tsai, Y. Wang, Y. Lai, H. Tsou, G. Liou, J. Ko, S. Wang, Kaempferol protects against propacetamol-induced acute liver injury through CYP2E1 inactivation, UGT1A1 activation, and attenuation of oxidative stress, inflammation and apoptosis in mice, Toxicol. Lett. 290 (2018) 97–109.

[31] M.N. BinMowyna, N.A. AlFaris, Kaempferol suppresses acetaminophen-induced liver damage by upregulation/activation of SIRT1, Pharm. Biol. 59 (2021) 144–154.

[32] J. Budzianowski, Kaempferol glycosides from *Hosta ventricosa*, Phytochemistry 29 (1990) 3643–3647.

[33] A.B. Durkeet, J.B. Harborne, Flavonol glycosides in *Brassica* and *Sinapis*, Phytochemistry 12 (1973) 1085–1089.

[34] P. Ranabahu, J.B. Harborne, The flavonoids of the genus *Lathyrus* and a comparison of flavonoid patterns within the tribe Vicieae, Biochem. Syst. Ecol. 21 (1993) 715–722.

[35] S. Chaouqi, N. Moratalla-López, G.L. Alonso, C. Lorenzo, A. Zouahri, N. Asserar, E.M. Haidar, T. Guedira, Effect of soil composition on secondary metabolites of Moroccan Saffron (*Crocus sativus* L.), Plants 12 (2023) 711.

[36] M.P. Repasky, R.B. Murphy, J.L. Banks, J.R. Greenwood, I. Tubert-Brohman, S. Bhat, R.A. Friesner, Docking performance of the glide program as evaluated on the Astex and DUD datasets: a complete set of glide SP results and selected results for a new scoring function integrating WaterMap and glide, J. Comput. Aided Mol. Des. 26 (2012) 787–799.

[37] A. Depeursingea, D. Racoceanub, J. Iavindrasanaa, G. Cohena, A. Platonc, P. Polettic, H. Müllera, Fusing visual and clinical information for lung tissue classification in HRCT data, Artif. Intell. Med 50 (2010) 13–21.

[38] P. Śledź, A. Caflisch, Protein structure-based drug design: from docking to molecular dynamics, Curr. Opin. Struct. Biol. 48 (2018) 93–102.

[39] A. Tiwari, Singh, Computational Approaches in Drug Designing, Bioinformatics, Elsevier, 2022, pp. 207–217.

[40] D.S. El-Agamy, Pirfenidone ameliorates concanavalin A-induced hepatitis in mice via modulation of reactive oxygen species/nuclear factor kappa B signalling pathways, J. Pharm. Pharmacol. 68 (2016) 1559–1566.

[41] H. Beard, A. Cholleti, D. Pearlman, W. Sherman, K.A. Loving, Applying physics-based scoring to calculate free energies of binding for single amino acid mutations in protein-protein complexes, PLoS One 8 (2013) e82849.

[42] I.M. Saur, R. Panstruga, P. Schulze-Lefert, NOD-like receptor-mediated plant immunity: from structure to cell death, Nat. Rev. Immunol. 21 (2021) 305–318.

[43] A.I. Khedr, G.A. Mohamed, S.R. Ibrahim, R.F. Abdelhameed, T.H. Shoaib, A.A. Alzain, K. Yamada, M.S. Refaey, Marihysin B, a new cyclic lipopeptide from culture broth of Staphylococcus sp.-antimicrobial and glucoamylase inhibitory activities, J. Mol. Struct. 1297 (2024) 137008.

[44] T.H. Shoaib, M.A. Almogaddam, Y.S. Andijani, S.A. Saib, N.M. Almaghrabi, A.F. Elyas, R.Y. Azzouni, E.A. Awad, S.G. Mohamed, G.A. Mohamed, Marine-derived compounds for CDK5 Inhibition in Cancer: integrating multi-stage virtual screening, MM/GBSA analysis and molecular dynamics investigations, Metabolites 13 (2023) 1090.

[45] G.A. Mohamed, A.M. Omar, M.E. El-Araby, S. Mass, S.R.M. Ibrahim, Assessments of alpha-amylase inhibitory potential of *Tagetes* flavonoids through *in vitro*, molecular docking, and molecular dynamics simulation studies, Int. J. Mol. Sci. 24 (2023) 10195.

[46] J.C. Shelley, A. Cholleti, L.L. Frye, J.R. Greenwood, M.R. Timlin, M. Uchimaya, Epik: a software program for pK a prediction and protonation state generation for drug-like molecules, J. Comput. Aided Mol. Des. 21 (2007) 681–691.

[47] W. Sherman, T. Day, M.P. Jacobson, R.A. Friesner, R. Farid, Novel procedure for modeling ligand/receptor induced fit effects, J. Med. Chem. 49 (2006) 534–553.

[48] J.J. Irwin, B.K. Shoichet, Docking screens for novel ligands conferring new biology: Mini perspective, J. Med. Chem. 59 (2016) 4103–4120.

[49] A. Dhasmana, S. Raza, R. Jahan, J.M. Lohani, J.M. Arif, High-throughput virtual screening (HTVS) of natural compounds and exploration of their biomolecular mechanisms: an *in-silico* approach, in: New Look to Phytomedicine, Elsevier, 2019, pp. 523–548.

[50] R.A. Friesner, J.L. Banks, R.B. Murphy, T.A. Halgren, J.J. Klicic, D.T. Mainz, M.P. Repasky, E.H. Knoll, M. Shelley, J.K. Perry Glide, A new approach for rapid, accurate docking and scoring. 1. Method and assessment of docking accuracy, J. Med. Chem. 47 (2004) 1739–1749.

[51] R.A. Friesner, R.B. Murphy, M.P. Repasky, L.L. Frye, J.R. Greenwood, T.A. Halgren, P.C. Sanschagrin, D.T. Mainz, Extra precision glide: docking and scoring incorporating a model of hydrophobic enclosure for protein− ligand complexes, J. Med. Chem. 49 (2006) 6177–6196.

[52] A.A. Alzain, F.A. Elbadwi, R.M. Mukhtar, T.H. Shoaib, N. Abdelmoniem, S.F. Miski, K.F. Ghazawi, M. Alsulaimany, S.G. Mohamed, B.E. Ainousah, Design of new Mcl-1 inhibitors for cancer using fragments hybridization, molecular docking, and molecular dynamics studies, J. Biomol. Struct. Dyn. (2023) 1–13.

[53] P. Banerjee, A.O. Eckert, A.K. Schrey, R. Preissner, ProTox-II: a webserver for the prediction of toxicity of chemicals, Nucleic Acids Res. 46 (2018) W257–W263.

[54] W. Huang, Y. Wang, X. Jiang, Y. Sun, Z. Zhao, S. Li, Protective effect of flavonoids from Ziziphus jujuba cv. Jinsixiaozao against acetaminophen-induced liver injury by inhibiting oxidative stress and inflammation in mice, Molecules 22 (2017) 1781.

[55] H. Lv, Q. Xiao, J. Zhou, H. Feng, G. Liu, X. Ci, Licochalcone A upregulates Nrf2 antioxidant pathway and thereby alleviates acetaminophen-induced hepatotoxicity, Front. Pharmacol. 9 (2018) 147.

[56] H. Li, Q. Weng, S. Gong, W. Zhang, J. Wang, Y. Huang, Y. Li, J. Guo, T. Lan, Kaempferol prevents acetaminophen-induced liver injury by suppressing hepatocyte ferroptosis via Nrf2 pathway activation, Food Funct. 14 (2023) 1884–1896.

[57] G.F. Asaad, H.M.I. Abdallah, H.S. Mohammed, Y.A. Nomier, Hepatoprotective effect of kaempferol glycosides isolated from *Cedrela odorata* L. leaves in albino mice: involvement of Raf/MAPK pathway, Res Pharm Sci. 16 (2021) 370–380.

[58] J. Li, Q. Lu, M. Peng, J. Liao, B. Zhang, D. Yang, P. Huang, Y. Yang, Q. Zhao, B. Han, Water extract from *Herpetospermum pedunculosum* attenuates oxidative stress and ferroptosis induced by acetaminophen via regulating Nrf2 and NF-κB pathways, J. Ethnopharmacol. 305 (2023) 116069.

[59] F. Jin, C. Wan, W. Li, L. Yao, H. Zhao Y. Zou, D. Peng, W. Huang, Formononetin protects against acetaminophen-induced hepatotoxicity through enhanced NRF2 activity, PLoS One 12 (2017) e0170900.

[60] H. Guo, J. Sun, D. Li, Y. Hu, X. Yu, H. Hua, X. Jing, F. Chen, Z. Jia, J. Xu, Shikonin attenuates acetaminophen-induced acute liver injury via inhibition of oxidative stress and inflammation, Biomed. 112 (2019) 108704.

[61] M. Elshal, M.E. Abdelmageed, Diacerein counteracts acetaminophen-induced hepatotoxicity in mice via targeting NLRP3/caspase-1/IL-1β and IL-4/MCP-1 signaling pathways, Arch Pharm. Res. (Seoul) 45 (2022) 142–158.

[62] A. Rousta, A. Shahmohammadi, Z. Mehrabi, S. Fallah, T. Baluchnejadmojarad, M. Roghani, Therapeutic potential of isorhamnetin following acetaminophen-induced hepatotoxicity through targeting NLRP3/NF-κB/Nrf2, Drug Res. 72 (2022) 245–254.

[63] C. Lee, S. Yoon, J.O. Moon, Kaempferol suppresses carbon tetrachloride-induced liver damage in rats via the MAPKs/NF-kappaB and AMPK/Nrf2 signaling pathways, Int. J. Mol. Sci. 24 (2023) 6900.

[64] A.S. Alshehri, A.F. El-Kott, M.S.A. El-Gerbed, A.E. El-Kenawy, G.M. Albadrani, H.S. Khalifa, Kaempferol prevents cadmium chloride-induced liver damage by upregulating Nrf2 and suppressing NF-kappaB and keap1, Environ. Sci. Pollut. Res. Int. 29 (2022) 13917–13929.

[65] Y. Xie, A. Ramachandran, D.G. Breckenridge, J.T. Liles, M. Lebofsky, A. Farhood, H. Jaeschke, Inhibitor of apoptosis signal-regulating kinase 1 protects against acetaminophen-induced liver injury, Toxicol. Appl. Pharmacol. 286 (2015) 1–9.

[66] Y. Xie, M.R. McGill, K. Dorko, S.C. Kumer, T.M. Schmitt, J. Forster, H. Jaeschke, Mechanisms of acetaminophen-induced cell death in primary human hepatocytes, Toxicol. Appl. Pharmacol. 279 (2014) 266–274.

[67] C. Saito, C. Zwingmann, H. Jaeschke, Novel mechanisms of protection against acetaminophen hepatotoxicity in mice by glutathione and N-acetylcysteine, Hepatology 51 (2010) 246–254.

[68] M. Wang, J. Sun, T. Yu, M. Wang, L. Jin, S. Liang, W. Luo, Y. Wang, G. Li, G. Liang, Diacerein protects liver against APAP-induced injury via targeting JNK and inhibiting JNK-mediated oxidative stress and apoptosis, Biomed. Pharmacother. 149 (2022) 112917.

[69] Y. Tian, F. Ren, L. Xu, X. Zhang, Distinct effects of different doses of kaempferol on D-GalN/LPS-induced ALF depend on the autophagy pathway, Mol. Med. Rep. 24 (2021) 682.

[70] E. Seki, D.A. Brenner, M. Karin, A liver full of JNK: signaling in regulation of cell function and disease pathogenesis, and clinical approaches, Gastroenterology 143 (2012) 307–320.

[71] S. Win, T.A. Than, J. Zhang, C. Oo, R.W.M. Min, N. Kaplowitz, New insights into the role and mechanism of c-Jun-N-terminal kinase signaling in the pathobiology of liver diseases, Hepatology 67 (2018) 2013–2024.

[72] X. Zhai, T. Dai, Z. Chi, Z. Zhao, G. Wu, S. Yang, D. Dong, Naringin alleviates a cetaminophen-induced acute liver injury by activating Nrf2 via CHAC2 upregulation, Environ. Toxicol. 37 (2022) 1332–1342.

[73] X. Zhan, J. Zhang, H. Chen, L. Liu, Y. Zhou, T. Zheng, S. Li, Y. Zhang, B. Zheng, Q. Gong, Capsaicin alleviates acetaminophen-induced acute liver injury in mice, Clin. Immunol. 220 (2020) 108578.

[74] T. Beringhelli, G. D'Alfonso, M. Freni, G. Ciani, M. Moret, A. Sironi, Synthesis and characterization of a family of nitrile-substituted triangular hydridocarbonyl rhenium clusters,[Re 3 (μ-H) 3 (CO) 12–n (NCMe) n](n= 1–3). X-Ray crystal structures of [Re 3 (μ-H) 3 (CO) 11 (NCMe)] and [Re 3 (μ-H) 3 (CO) 9 (NCMe) 3], J. Chem. Soc. Dalton Trans. (1989) 1143–1148.

[75] Y. Shimizu, T. Yonezawa, J. Sakamoto, T. Furuya, M. Osawa, K. Ikeda, Identification of novel inhibitors of Keap1/Nrf2 by a promising method combining protein–protein interaction-oriented library and machine learning, Sci. Rep. 11 (2021) 7420.

[76] E. Jnoff, C. Albrecht, J.J. Barker, O. Barker, E. Beaumont, S. Bromidge, F. Brookfield, M. Brooks, C. Bubert, T. Ceska, Binding mode and structure–activity relationships around direct inhibitors of the Nrf2–Keap1 complex, ChemMedChem 9 (2014) 699–705.

[77] F. Chen, K. Beezhold, V. Castranova, JNK1, a potential therapeutic target for hepatocellular carcinoma, BBA Rev. Cancer. 1796 (2009) 242–251.

[78] I. Nikolic, M. Leiva, G. Sabio, The role of stress kinases in metabolic disease, Nat. Rev. Endocrinol. 16 (2020) 697–716.

[79] X. Xie, Y. Gu, T. Fox, J.T. Coll, M.A. Fleming, W. Markland, P.R. Caron, K.P. Wilson, M.S. Su, Crystal structure of JNK3: a kinase implicated in neuronal apoptosis, Structure 6 (1998) 983–991.

[80] S. Baek, N.J. Kang, G.M. Popowicz, M. Arciniega, S.K. Jung, S. Byun, N.R. Song, Y. Heo, B.Y. Kim, H.J. Lee, Structural and functional analysis of the natural JNK1 inhibitor quercetagetin, J. Mol. Biol. 425 (2013) 411–423.

[81] M.T.H. Duong, J. Lee, H. Ahn, C-Jun N-terminal kinase inhibitors: structural insight into kinase-inhibitor complexes, Comput. Struct. Biotechnol. J. 18 (2020) 1440–1457, 2020.

[82] V. Oza, S. Ashwell, L. Almeida, P. Brassil, J. Breed, C. Deng, T. Gero, M. Grondine, C. Horn, S. Ioannidis, Discovery of checkpoint kinase inhibitor (S)-5-(3-fluorophenyl)-N-(piperidin-3-yl)-3-ureidothiophene-2-carboxamide (AZD7762) by structure-based design and optimization of thiophenecarboxamide ureas, J. Med. Chem. 55 (2012) 5130–5142.

[83] J.T. Liles, B.K. Corkey, G.T. Notte, G.R. Budas, E.B. Lansdon, F. Hinojosa-Kirschenbaum, S.S. Badal, M. Lee, B.E. Schultz, S. Wise, ASK1 contributes to fibrosis and dysfunction in models of kidney disease, J. Clin. Invest. 128 (2018) 4485–4500.